Oxygen Activation in Neuronal NO Synthase: Resolving the Consecutive Monooxygenation Steps

Citation for published version:
Papale, D, Bruckmann, C, Gazur, B, Miles, CS, Mowat, CG & Daff, S 2012, 'Oxygen Activation in Neuronal NO Synthase: Resolving the Consecutive Monooxygenation Steps' Biochemical Journal, vol. 443, no. 2, pp. 505-514. DOI: 10.1042/BJ20111644

Digital Object Identifier (DOI):
10.1042/BJ20111644

Link:
Link to publication record in Edinburgh Research Explorer

Document Version:
Peer reviewed version

Published In:
Biochemical Journal

Post-print of a peer-reviewed article published by Portland Press Ltd. – a wholly owned subsidiary of the Biochemical Society.
The final version of record is available at: http://dx.doi.org/10.1042/BJ20111644

Cite as:
Papale, D., Bruckmann, C., Gazur, B., Miles, C. S., Mowat, C. G., & Daff, S. (2012). Oxygen Activation in Neuronal NO Synthase: Resolving the Consecutive Monooxygenation Steps. *Biochemical Journal*, 443(2), 505-514.

Manuscript received: 12/09/2011; Revised: 17/01/2012 Accepted & published: 03/02/2012

Oxygen activation in neuronal NO synthase: Resolving the consecutive mono-oxygenation steps**

Davide Papale, Chiara Bruckmann, Ben Gazur, Caroline S. Miles, Christopher G. Mowat and Simon Daff*

EaStCHEM, School of Chemistry, Joseph Black Building, University of Edinburgh, West Mains Road, Edinburgh, EH9 3JJ, UK.

[*]Corresponding author; email: Simon.Daff@ ed.ac.uk, tel.: +44 131 6507378, fax: +44 131 6504760

[**]The research was performed with support from the BBRSC [Grant No. C17500], The Royal Society, through a University Research Fellowship to SD and The Leverhulme Trust [Grant No. F/00158/CG]. We thank ESRF BM14 Grenoble for the use of synchrotron facilities, Prof. S.K. Chapman, Prof. J.C. Fontecilla-Camps and X. Vernede for assistance, L. Campbell for help in preparing the manuscript and Prof. T. Shimizu for supplying the $nNOS_{oxy}$ expression plasmid.

Supporting information:
The atomic co-ordinates for the G586S $nNOS_{oxy}$ mutant have been deposited in the PBD under code 3FC5.

Abbreviations:
The abbreviations used are: P450, cytochrome P450 monooxygenase; SHE, standard hydrogen electrode; nNOS, neuronal nitric oxide synthase; $nNOS_{oxy}$, the nNOS oxygenase domain; H_4B, tetrahydrobiopterin; aH_4B, 4-amino-tetrahydrobiopterin; NOHA, N-γ-hydroxy-L-arginine; PMSF, phenylmethylsulfonyl fluoride; OTTLE, Optically Transparent Thin Layer Electrode; SDS, sodium dodecyl sulphate; L-NAME, N-γ-nitro-L-arginine methyl ester; L-NIO, N5-(1-iminoethyl)-L-ornithine; SOD, Superoxide Dismutase; DTT, Dithiothreitol; BSA, Bovine Serum Albumin.

Keywords:
Oxygen activation; NOS; tetrahydrobiopterin; electron transfer; Kinetics; proton transfer

Abstract

The vital signalling molecule nitric oxide is produced by mammalian NOS enzymes in two steps. L-arginine is converted to N-hydroxy-L-arginine NOHA, which is converted to NO and citrulline. Both steps are thought to proceed via similar mechanisms in which the cofactor tetrahydrobiopterin (H_4B) activates dioxygen at the heme site by electron transfer. The subsequent events are poorly understood due to the lack of stable intermediates. By analogy with cytochromes P450, a heme-iron oxo species may be formed, or direct reaction between a heme-peroxy intermediate and substrate may occur. The two steps may also occur via different mechanisms. Here we analyse the two reaction steps using the G586S mutant of nNOS, which introduces an additional H-bond in the active site and provides an additional proton source. In the mutant, H_4B activates dioxygen as in the wild-type enzyme, but an interesting intermediate heme species is then observed. This may be a stabilized form of the active oxygenating species. The mutant is able to perform step 2 (reaction with NOHA), but not step 1 (with L-Arg) indicating that the extra H-bond enables it to discriminate between the two monooxygenation steps. This implies that the two steps follow different chemical mechanisms.

Introduction

The mammalian nitric oxide synthases (NOS) produce NO to act as a signalling agent in the cardiovascular and nervous systems and as part of the immune response. NO production is highly regulated and is involved in numerous disease states, including neurodegenerative diseases, hypertension, cardiovascular disease, impotence and septic shock. They are large multidomain enzymes with a unique structure and chemical mechanism. The latter has medical, biological and chemical significance, and is the subject of this paper.

The NO synthases catalyze NO production from L-Arg in two consecutive steps [1-4]. The first step leads to the production of N^G-hydroxy-L-arginine (NOHA), a stable enzyme-bound intermediate, while the second results in the production of NO and L-citrulline (Scheme 1). Each step consumes a molecule of dioxygen, which binds to a ferrous heme group at the catalytic site and is activated by reductive electron transfer. The heme is thiolate ligated like a cytochrome P450, but the NO synthases share few other structural similarities with this class of enzyme [5, 6], although the electrons required for catalysis are supplied by a reductase domain, which is related in both structure and function to mammalian cytochrome P450 reductase [7, 8]. The fact that P450s and NOS share similar cofactors, reductases and oxygen activation steps has led to speculation that their chemical mechanisms are related. While this is justified, the differences between the two enzyme classes are also likely to influence the catalytic pathway. Firstly, NOS binds a molecule of tetrahydrobiopterin (H_4B), which hydrogen-bonds to one of the heme propionates in the active site [5, 6]. H_4B acts as an electron transfer cofactor and, uniquely, supplies the second electron required for oxygen activation in both steps of the NO synthesis reaction [2]. In the second step, the H_4B radical cation thus formed is also required to reclaim an electron from the ultimate ferrous nitrosyl complex to facilitate NO release [2, 9, 10]. Secondly, the NOS active site is hydrophilic and binds a positively charged substrate. The monooxygenation of a guanidinium group is not a usual P450-type reaction. Thirdly, the thiolate ligand to the NOS heme is hydrogen bonded to a tryptophan residue (W409 in rat nNOS), which stacks below the heme plane. An additional tryptophan residue contacts the heme at the back of the active site. These may play some role in radical stabilisation and influence the properties of the ligating cysteinyl ligand [5, 6, 11, 12]. Despite these differences, the P450 monooxygenation reaction is a good starting point for discussing the chemistry of NO synthesis.

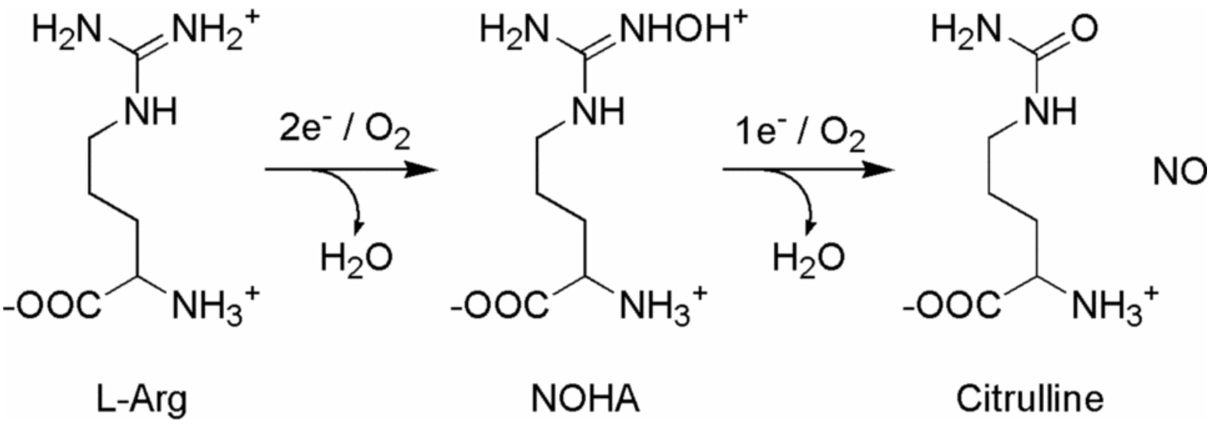

Scheme 1. NO synthesis from L-arginine

There are two main mechanistic ideas for P450-dependent monooxygenation; either the substrate reacts directly with a ferric hydroperoxo-heme complex or this decays on protonation to form a compound I oxyferryl heme radical cation, which then abstracts a hydrogen atom from the substrate. These mechanisms have been discussed at length in numerous reviews, with the latter being favoured in most circumstances [13-16]. To gain further insight into the mechanism, it is necessary to trap intermediates on the reaction pathway. The last stable intermediate to be observed in both the P450 and NOS reactions is the oxyferrous heme complex. One-electron reduction of this must yield a peroxo-heme species, but this and subsequent intermediates are too unstable to accumulate under normal circumstances, although the compound I species of a thermostable P450 has been observed in stopped-flow experiments with m-chloroperbenzoic acid [17, 18]. Cryoreduction of the oxyferrous substrate complex of P450cam at 77 K followed by EPR and ENDOR analysis led Davydov *et al.* [19] to observe a ferric peroxo-heme species, which undergoes protonation to form a hydroperoxoferric species. The next species observed was a product-heme complex. In a parallel study of the NOS reaction [20] a similar peroxoferric heme complex was observed in the presence of L-Arg, which decayed to form a product-heme complex in which the hydroxyl group of NOHA was thought to be coordinated to the ferric heme iron. In both cases the formation of a compound I species as an intermediate was implied by the direct coordination of product to the heme iron in the final complex. Using the *G. stearothermophilus* NOS, the same group followed the reaction a stage further to observe protonation of the peroxoferric heme complex prior to reaction. The reaction with NOHA as substrate did not follow the same course however, leading the authors to propose different reactive intermediates for the two stages of NO synthesis. Although it is known that H_4B transfers an electron to the oxyferrous heme species during oxygen activation [2, 9, 10] [21-23] to form a peroxo-heme complex, the subsequent reactions are uncertain. The first step of the NOS reaction and the second may also follow different mechanisms [1, 3, 24].

In this paper we report how the G586S mutation of nNOS introduces an additional hydrogen bond to the substrate in the active site of the enzyme, as demonstrated by stronger substrate binding and an X-ray crystal structure. Pre-steady-state kinetics show that the mutation alters the H_4B-driven oxygen activation process in the presence of L-Arg, by stabilising an unusual heme-oxy species. Single turnover analysis indicates that the substrate L-Arg is not transformed to product during this process, however the intermediate NOHA is. The results demonstrate the influence of H-bonding and proton transfer in this important and fascinating catalytic mechanism.

Experimental Procedures

Chemicals were purchased from Sigma-Aldrich (Poole, Dorset) except where differently stated.

Mutagenesis: The G586S mutant was generated by site-directed mutagenesis of the pCWori plasmid previously used for expression of the nNOS oxygenase domain [23, 25], using the Kunkel method [26]. The oligonucleotides for site-directed mutagenesis were ordered from MGW-Biotech. The forward primer, CCTGTCCCTTCAGCAGCTGGTACATGGGC, was used, and a complementary sequence for the reverse primer.

Enzyme preparation: Wild type and mutant nNOS oxygenase domains ($nNOS_{oxy}$, residues 1–720 with an N-terminal His tag) were purified as described previously [25] from *E. coli* BL21 cells containing pCWori (NOS) and pGroESL expression plasmids. The cells were lysed in 50 mM Tris-HCl (pH 7.5), containing 0.5 mM EDTA, 10% glycerol, 20 μM H_4B (Schircks Lab., Switzerland) 1 mM dithiothreitol, 25 mM phenylmethylsulfonyl fluoride (PMSF), 20 mM imidazole, 0.1 mM L-arginine, 0.3 M NaCl and a protease inhibitor tablet for every 50 ml of buffer (Complete, Roche Applied Science) and centrifuged for 1 hour at 20,000 x *g*. The supernatant was applied to a nickel agarose 5 ml prepacked column (HisTrap HP, Amersham Biosciences), linked to a FPLC system (Åkta Purifier), washed with 5 column volumes of lysis-buffer . It was then eluted with the same buffer containing 150 mM imidazole. The enzyme fractions were concentrated to 5 ml and loaded onto a G25 size exclusion column to remove imidazole. The protein solution was collected, concentrated again and flash frozen in $N_{2(l)}$. To prepare aH_4B-bound enzyme, 20 µM 4-amino-H_4B (Schircks Laboratory) replaced H_4B in the purification buffers. Enzyme samples were >90% pure according to SDS-PAGE. The concentration of nNOS$_{oxy}$ was quantified optically using ferrous CO difference spectrum, $\Delta\varepsilon$(444–467 nm) = 55 mM^{-1} cm^{-1} [27]. Enzyme solutions for crystal growth were dialyzed against HEPES 50mM (pH 7.5), 10 % glycerol, 0.1 mM L-arginine, 20 µM H_4B, 1 mM dithiothreitol, 0.25 mM PMSF and loaded onto a Resource Q column. Elution was performed with the same buffer containing 0.3 M NaCl after which the protein was concentrated to 300 µM and flash frozen in $N_{2(l)}$.

nNOS$_{oxy}$ peroxide shunt assays: Nitrite production by wild-type and G586S nNOS$_{oxy}$ was determined using the Greiss reagents sulfanilamide and *N*-(1-naphthyl)ethylenediamine following the peroxide shunt assay [28, 29]. The product of the Griess reaction, a pink azo-dye, was measured by taking the absorbance at 540nm. The assay mix consisted of a 100µl reaction mixture prepared in 50mM Tris buffer pH7.5 with either 250nM nNOS$_{oxy}$ WT or nNOS$_{oxy}$ G586S, 0.1-1000 µM H_4B, 1mM NOHA, 0.5mM DTT, 10units/ml SOD and 0.5mg/ml BSA. The reaction was initiated by the addition of hydrogen peroxide added to a final concentration of 30mM. The reaction was incubated at 25˚C for 10 mins and quenched with the addition of 1500 units of catalase.

Titrations: Difference spectrophotometry titrations were conducted to quantify the affinities of substrates, substrate-analogues and diatomic molecules. Optical spectra were recorded using a UV-1601 Shimadzu spectrophotometer at 20 °C. 1 ml solutions of nNOS$_{oxy}$ were prepared in a cuvette in 50 mM Tris (pH7.5). Standard solutions of substrates and other compounds were prepared at high concentration in the same buffer and sequentially added having a final change in the sample volume of less than 5%. Manipulation of the spectra obtained was performed to determine the dissociation constants (K_d). Briefly: from each spectrum the substrate-free enzyme spectrum was subtracted. The absorbance difference between two evident peaks was determined, and the values plotted against substrate concentration. K_d values were determined by fitting to a rectangular hyperbola. In the cases where the affinity of the compound appeared to be extremely high (L-Arg with the G586S mutant) imidazole was used as a competitive heme ligand [30]. The formula: $K_{d\ apparent} = K_d (1+[imidazole]/K_{imidazole})$ was used to calculate K_d values extrapolated to zero imidazole concentration.

Pre-steady-state Kinetics: Stopped flow single-wavelength and diode-array experiments were performed at 10 °C using an Applied Photophysics stopped-flow spectrophotometer (SX.17MV) in an anaerobic glove box (Belle Technology; [O_2] < 5 ppm) [23]. Enzyme solution was in 50 mM Tris/HCl, pH 7.5, with the addition of either 10 μM H_4B or 10 μM aH_4B in excess over the enzyme concentration. Substrates were present at a concentration of 10 mM when required. $nNOS_{oxy}$ wild type or G586S at 10 μM was chemically reduced through the addition of sodium dithionite in a slight stoichiometrical excess. Excess sodium dithionite was removed on a pre-equilibrated 10 ml G25 gel filtration column. The $nNOS_{oxy}$ ferrous state was verified by recording the UV-Vis spectrum on a Varian Cary 50 Bio spectrophotometer also contained in the anaerobic box. Different concentrations of oxygen were obtained through the dilution of oxygen-saturated buffer: the O_2 concentration was measured by exploiting the absorbance change caused by oxidation of electrochemically reduced methyl viologen (ϵ_{600} = 13,000 $M^{-1}cm^{-1}$) [23]. Formation of the oxyferrous complex was monitored after mixing ferrous enzyme and oxygen through changes to the UV-Vis spectrum. Rate constants (k_{obs}) for oxyferrous complex formation were obtained by fitting the traces observed at 426 nm to a single exponential function. Each k_{obs} was then plotted against the corresponding oxygen concentration: the slope obtained through linear regression fitting was interpreted as a second order rate constant (k_{2nd}) for oxyferrous complex formation in the various conditions. Oxy-ferrous complex decay on the other hand, being in most of the cases independent from oxygen concentration, was determined by fitting each trace at 390 nm for different oxygen concentrations to a single exponential function and averaging the resultant rate constants (k_{decay}). Diode array data for each set of conditions were also analysed globally using the vendor's software (Pro-Kineticist 4.21, Applied Photophysics) and models consisting of either two or three consecutive steps. The spectra of the intermediates accumulating and their concentration timecourses were determined.

Single Turnover Analysis: The products of the reaction of $nNOS_{oxy}$ and L-arg or NOHA with dioxygen were determined essentially by the method of Abu-Soud *et al.* [31]. Several 1 ml samples of 50μM reduced H_4B-bound enzyme were exchanged into 50mM Hepes buffer, 0.1M NaCl, 1μM H_4B, pH 7.5 in an anaerobic glovebox and to each was added either L-arg or NOHA to a concentration of 150μM. These were then exposed to air for several minutes. The reaction solutions were then separated from the protein by centrifuging in Millipore filters with 10000 MW cutoffs. For each sample, 80 μl of filtrate was mixed with 20μl of OPA reagent (1 mM *o*-phthaldialdehyde, 10 v/v methanol, 1 v/v β-mercaptoethanol) for 1 minute immediately before use in HPLC. After derivatisation a 10μl sample was injected onto a Phenomenex Luna 250 x 10.00 mm column, 5 micron particle size. The column was eluted under the following conditions. Buffer A= 5% acetonitrile, 15mM sodium borate with 0.1 v/v trifluoracetic acid, pH 9. Buffer B= 50% acetonitrile, 8mM sodium borate, 0.1 v/v trifluoroacetic acid, pH 9. The solvent gradients were linear and as follows; Flow rate 1.5 ml/min. 0-10 min= 0-12% buffer B. 15-26 min= 12-85% buffer B. 31-36 min= 85-0% buffer B. OPA-derivatised citrulline, NOHA and arginine eluted at 30.7, 31.0, and 32.1 min respectively as easily resolved peaks. Fluorescence was detected by excitation at 360nm and emission at 455nm using a Gilson 122 fluorometer. Each reaction was run in duplicate and each reaction analysed in duplicate.

Optically Transparent Thin Layer Electrode (OTTLE) Potentiometry: To determine G586S $nNOS_{oxy}$ heme reduction potential, electrochemical potentiometry experiments were performed using a modified quartz EPR cell with a path length of 0.3 mm and provided with three electrodes: the gauze-like working electrode (Pt/Rh, 95/5), a Pt wire as a counter electrode and an Ag/AgCl reference electrode [12, 23]. Enzymes aliquots of 0.5 ml were passed through a G-25 column pre-equilibrated with 0.1 M Tris pH 7.5, 0.5 M KCl, 10 μM H_4B in an anaerobic box. Mediators to facilitate the electron transfers were added: pyocyanine (10 μM) 2 hydroxy-1,4-napthoquinone (20 μM), FMN (5 μM), benzyl viologen (10 μM) and methyl viologen (10 μM). The potentials of the electrodes were controlled through Autolab PGSTAT10 potentiostat 6 and spectra to monitor the redox state of the enzyme were taken periodically using a Cary 50 UV/vis spectrophotometer. At a controlled temperature of 25 ± 2 °C the working electrode potentials were decreased stepwise (30 mV) and the enzyme solution allowed to equilibrate until no current was detected. This was repeated until the enzyme was completely in the ferrous form and then back until completely to the ferric form. Absorbance changes were interpreted as the transformation of the enzyme into the two different redox states and then plotted against the applied potentials. The points were fitted using Nernst equation and the midpoint at which the enzyme is partitioned 50% in each redox state interpreted as the heme reduction potential. All electrode potentials were corrected according to the standard hydrogen electrode.

X-ray Crystallography: Crystallization of G586S $nNOS_{oxy}$ was carried out by hanging drop or sitting drop vapour diffusion in an anaerobic glove box (Belle Technology, $[O_2] < 5$ ppm) at 18 °C. Crystals were obtained with well solutions comprising 100 mM NaMES buffer (pH 5.8 – 6.0), 200 mM ammonium acetate, 25 mM L-arginine, 35 μM sodium dodecyl sulfate (SDS), 5 mM glutathione, 2 % isopropanol and 22-24 % (w/v) PEG 3350. Drops of 4 μl volume were prepared by adding 2 μl of 7-9 mg/ml protein (in 50 mM Tris-HCl pH 7.8, 10 % glycerol, 10 mM dithiothreitol, 20 μM H_4B, 0.1 mM L-arginine and 200 mM NaCl) to 2 μl of well solution. After 24 hours small rod-shaped crystals appeared which reached maximum size (~100 μm in length) after ~7 days. Prior to flash-cooling in liquid propane crystals were exposed to a cryoprotectant solution in a step-wise fashion, with the final cryoprotectant solution comprising 25 % (w/v) PEG 3350, 100 mM NaMES buffer pH 5.8-6.0, 100 mM ammonium acetate, 10 % (v/v) glycerol, 10 % (w/v) trehalose, 5 % (w/v) sucrose, 5 % (w/v) mannitol and 1 mM L-arginine. A data set was collected to 2.6 Å resolution at ESRF in Grenoble (beamline BM14; $\lambda = 0.9737$ Å) using a Mar Research CCD detector. Crystals were found to belong to space group $P2_12_12_1$ with cell dimensions $a = 51.963$ Å, $b = 110.847$ Å and $c = 164.627$ Å. Data processing and molecular replacement was carried out using the CCP4 package [32]. The wild-type

$nNOS_{oxy}$ structure (PDB ID 1OM4), stripped of water, was used as the initial model for molecular replacement. Electron density fitting was carried out using the programs TURBO-FRODO and COOT [33]. Structure refinement was carried using PHENIX [34]. The atomic coordinates have been deposited in the Protein Data Bank, entry 3FC5.

Results

Titrations: The UV/visible spectrum of G586S nNOSoxy was found to be very similar to that of the wild-type enzyme. The oxidised mutant had a broad Soret absorption band at around 400 nm attributed to mixed spin ferric heme. This shifted on addition of substrate to 390 nm, indicating conversion to the high-spin ferric state. The change in spectrum was used to determine dissociation constants (Table 1) for various substrates and analogues (Figure S10). The first thing to note was the increased affinity of the mutant for L-Arg, the K_d for which decreased by 10-fold on mutation to 0.1 μM. This is typical of a shift in binding affinity induced by an additional hydrogen-bonding interaction between protein and substrate. The K_d for NOHA also decreased, but only by half, indicating that the interaction is weaker with the intermediate substrate. In the crystal structure of the complex between NOHA and nNOS, the N-hydroxy group occupies the space adjacent to G586 and is therefore likely to be impeded by the mutation of this residue [35].

	G586S **K_d (μM)**	**Wild Type** **K_d (μM)**
L-Arg	0.10 ± 0.05†	1.0 ± 0.1
NOHA	0.5 ± 0.1	0.9 ± 0.1
Imidazole	235 ± 4	86 ± 2
Agmatine	42.8 ± 5.7	130 ± 23.5
Amino Guanididne	546 ± 70	1530 ± 77
L-NAME	31.7 ± 2.0	7.9 ± 3.3
L-NIO	11.4 ± 0.6	2.7 ± 0.7

† Measured by competition with imidazole.

Table 1. Dissociation Constants (K_d) for nNOS Substrates and Substrate-Analogues; Comparison of nNOS Wild-Type and G586S mutant.

The dissociation constants for the substrate-analogues were found to form two distinct groups. Agmatine and aminoguanidine had 3-fold higher affinity for the mutant than the wild-type enzyme, whereas N(G)nitro-L-arginine methyl ester (L-NAME) and N5-(1-iminoethyl)-L-ornithine (L-NIO) had 4-fold lower affinity. The results show that the analogues with an unsubstitued guanidinium group (like L-Arg) bind more tightly to the mutant, whereas those with modified guanindinium groups bind less well. Clearly, the newly introduced Ser residue forms a favourable hydrogen-bond with the guanidinium group and increases the selectivity of the active site for this.

***$nNOS_{oxy}$* peroxide shunt assays:** Wild type and G586S $nNOS_{oxy}$ were tested for their ability to produce nitric oxide from NOHA using the peroxide shunt assay [28, 29]. Both enzymes reached their maximum catalytic rate in the presence of a stoichiometric amount of H_4B and had similar concentration dependencies. Under these conditions wild-type and G586S $nNOS_{oxy}$ produced 0.142 ±0.011 and 0.154 ±0.005 nmol of nitrite per nmol enzyme respectively in 10 min assays as measured using the Greiss reaction. In these assays, nitrite results from the production of NO, indicating that the mutant is as catalytically competent as the wild-type enzyme in performing nitric oxide synthesis via this reaction.

***Single turnover of ferrous $nNOS_{oxy}$*:** Wild type and G586S $nNOS_{oxy}$ were tested for their ability to produce NOHA from arginine, and citrulline from NOHA in single turnover reactions. OPA derivatives of all three amino acids were resolved and measured by HPLC fluoroscopy allowing monitoring of conversion by single turnover using pre-reduced enzyme. Both proteins proved capable of converting NOHA to citrulline. However the G586S mutant proved unable to convert arginine to NOHA under these conditions, while the wild type protein was fully competent, see supplementary Figures S7-S9. While the OPA derivatisation method here described is not suited to absolute quantification, the results are qualitatively unambiguous. The ability of the G586S mutant to catalyse the second monooxygenation but not the first indicates that the extra H-bond selectively inhibits the latter, indicating an important mechanistic difference between the two steps.

***$nNOS_{oxy}$* G586S reduction potentials:** In order to assess whether the G586S mutation affects the reduction potential of the heme, spectroelectrochemical analysis was conducted using an OTTLE cell (Table 2). Midpoint potentials for the heme in the presence and absence of L-Arg were found to be within 15 mV of the wild-type enzyme [23] and largely within experimental error. It is unlikely that this shift would have a significant effect on the properties of the enzyme and indicates that the fundamental electronic properties of the heme centre are similar in the mutant and wild-type enzyme.

	No substrate	**L-Arg**
G586S (mV)	-329±8	-318±4
wt (mV) †	-316±5	-306±4

† Taken from Ost and Daff [23]

Table 2. Reduction Potentials of $nNOS_{oxy}$ Wild Type and G586S Mutant in the Presence and Absence of L-Arginine.

Stopped Flow analysis of Oxy-Ferrous compound formation and decay: Stopped flow spectroscopy was used to study the formation and decay of the oxyferrous complex of G586S nNOSoxy on rapid mixing of the ferrous enzyme with oxygen-saturated buffer in an anaerobic chamber. Variation of the oxygen concentration enabled the second order rate-constant for oxygen binding to be determined (Table 3). For the mutant enzyme in the presence of substrate, the rate constant was found to be up to 3-fold higher than for the wild-type enzyme. This may indicate a strengthening of the interaction of heme-bound dioxygen with the substrate in the active site. In the absence of substrate, the formation of a discrete oxyferrous complex could not be observed and the second-order rate constant for enzyme oxidation was 30-fold lower, indicating that oxygen binds weakly to the mutant enzyme in the absence of substrate. A similar effect is observed in the wild-type enzyme, where substrate increases the rate of oxygen binding and the stability of the oxyferrous complex [23], but it is much less pronounced in this case. The distance between the mutated residue and the oxygen binding site is too large for the Ser to block oxygen binding. Therefore, the most likely cause of the disruption is modification of the hydrogen-bonding network among water molecules within the active site. For example, the stabilisation of bound water molecules in the vicinity of the heme iron through hydrogen-bonding would disfavour dioxygen binding.

	Substrate	**Oxy-ferrous formation** $\boldsymbol{k_{2nd}}$ **(μM^{-1} s^{-1})**
Wild type†	**-**	0.46 ± 0.10
	L-Arg	1.1 ± 0.1
	NOHA	1.1 ± 0.1
G586S	**-**	0.10 ± 0.01
	L-Arg	2.8 ± 0.2
	NOHA	3.1 ± 0.2

† Taken from Ost and Daff [23]

Table 3. Second-Order Rate Constants for Formation the Oxy-ferrous Complexes of $nNOS_{oxy}$ Wild Type and G586S Mutant.

The rate of decay of the oxyferrous complex of NOS (Table 4) is highly dependent on the interaction of bound dioxygen with substrate, and on the presence of H_4B [23]. In some of these experiments H_4B was substituted with 4-amino-H_4B (aH_4B) to retain the dimeric structure of the enzyme, but to remove the electron transfer capability of the cofactor [23, 36]. For the G586S mutant in the absence of substrate, the oxyferrous complex does not accumulate due to weak oxygen binding, so the decay kinetics could not be studied further, even in the presence of aH_4B. In the presence of L-Arg and aH_4B the oxyferrous complex decays in a single exponential phase at 0.089 s^{-1}; slightly faster than for the wild-type enzyme. This most likely represents the rate of superoxide dissociation from the heme iron and indicates a similar oxyferrous complex stability. In the presence of H_4B, electron transfer from the biopterin to the oxyferrous complex triggers much faster decay due to either peroxide release in the absence of substrate, or reaction with substrate if present [23]. For the wild-type enzyme in the presence of L-Arg this occurs in a single kinetic phase resulting in formation of the high-spin ferric heme complex at 47 s^{-1} and the production of NOHA in the active site. For the G586S mutant a significant deviation from this reaction is observed (Figure 1). The oxyferrous complex formed by the mutant in the presence of L-Arg had a Soret peak at 436 nm, which is significantly red-shifted with respect to the wild-type enzyme (429 nm). Interestingly, the oxyferrous complex formed by G586S nNOSoxy in the presence of aH_4B was not red-shifted and appeared to be the same as for the wild-type enzyme. This indicates that the native cofactor (H_4B) induces the spectral shift. The oxyferrous complex decayed in two clearly distinct kinetic phases with rate-constants of 18 s^{-1} and 1.1 s^{-1} to the high-spin ferric heme complex. The first decay is not observed in the presence of aH_4B and must therefore require the native cofactor to trigger the reaction by electron transfer. The UV/vis spectrum of the intermediate formed during this biphasic decay process was determined by fitting the time-dependent spectral changes using global analysis software to a 3-step kinetic model, in which the sequential steps are oxyferrous complex formation, intermediate formation and decay to ferric heme. The three distinct phases can also be observed by looking at two different wavelengths (see Figure 2). At 408 nm conversion of ferrous enzyme to the oxyferrous complex is observed as a very fast exponential decay. This is followed by a slow increase as the ferric heme resting state builds up. At 423 nm an additional phase is observed showing conversion of the oxyferrous complex to the intermediate. The kinetic data fit extremely well to the three-step model used in global analysis and the results are unambiguous (see supplementary Figure S5). The spectrum of the intermediate (Figure 3) is very different to that of other NOS_{oxy} heme complexes and cannot be recreated by linear combination of any of these. It has a broad Soret band with a maximum at 421 nm and a shoulder at approximately 350 nm. There is very little definition in the 500 to 600 nm range where α and β bands common to heme proteins usually appear, and there is an increase in absorbance in the 700 nm region of the spectrum, which appears as a rise in the absorption baseline during formation and a decrease during decay.

			Oxy-ferrous decay k_{decay} (s^{-1})	
Wild type	**Amino-H_4B**	**L-Arg**	0.065 ± 0.010	**-**
	H_4B	**L-Arg**	47 ± 2	**-**
	H_4B	**NOHA**	22.5 ± 0.5	4.9 ± 0.5†
G586S	**Amino-H_4B**	**L-Arg**	0.089 ± 0.02	**-**
	H_4B	**L-Arg**	18 ± 2	1.1 ± 0.1
	H_4B	**NOHA**	11 ± 2	0.8 ± 0.1

† NO dissociation rate constant

Table 4. Rate Constants for Decay of the Oxy-ferrous Complexes of Wild Type and G586S $nNOS_{oxy}$ Determined by Global Analysis.

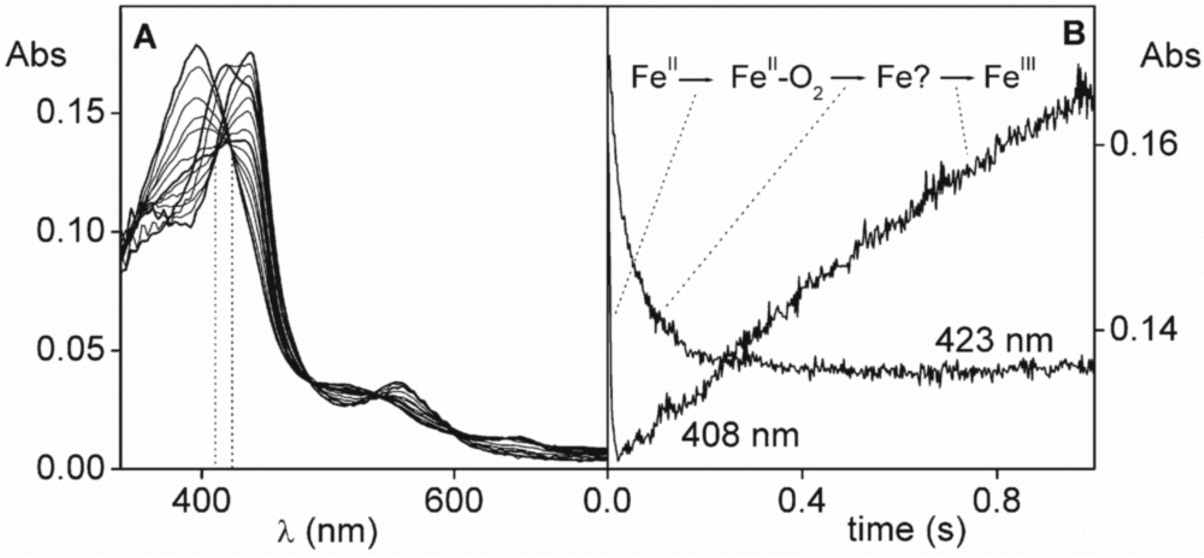

Figure 1. Pre-steady-state Reaction of G586S nNOS$_{oxy}$ with Oxygen in the Presence of L-Arginine and H$_4$B. Stopped flow diode array spectra are shown left, and single wavelength traces at 408 nm and 423 nm illustrating 3 distinct kinetic phases are shown right.

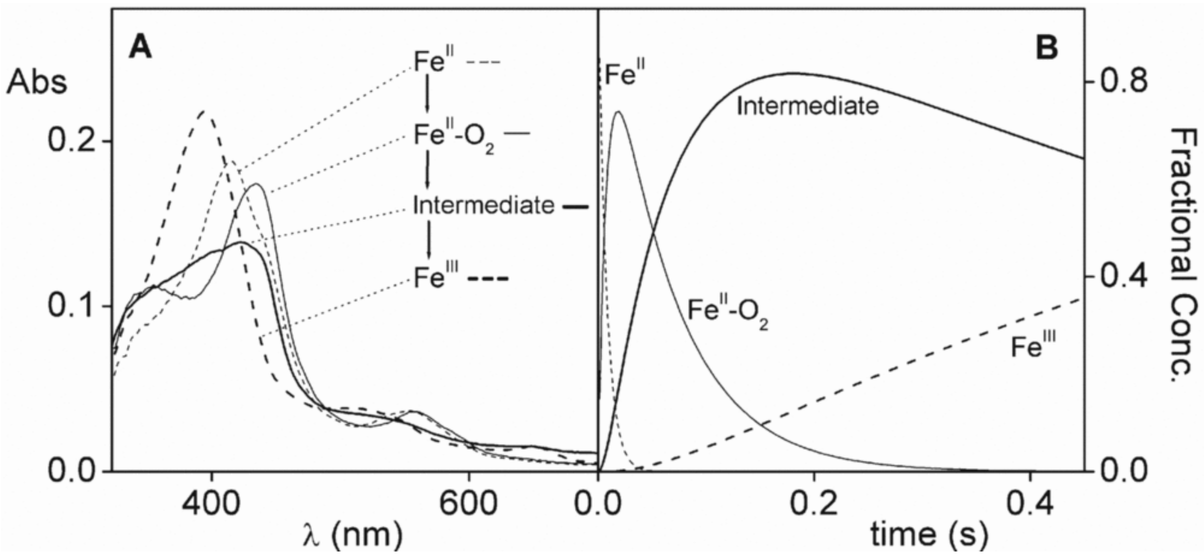

Figure 2. Global Analysis of the Pre-steady-state Reaction of G586S nNOS$_{oxy}$ with Oxygen in the Presence of L-Arginine and H$_4$B Using an A→B→C→D kinetic model. Spectral intermediates are shown left and intermediate time courses right.

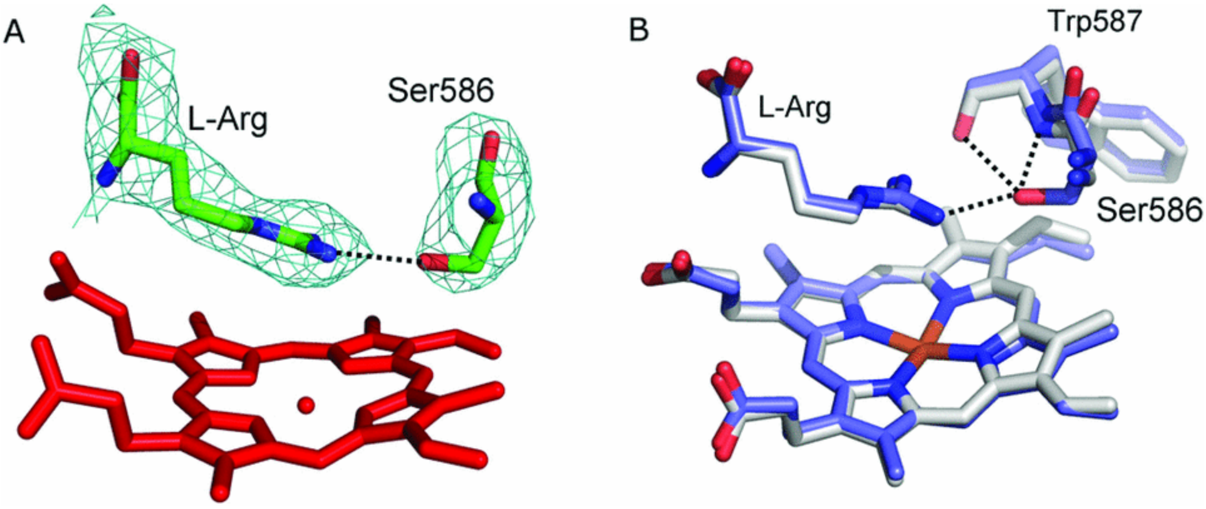

Figure 3. (A) Electron density around the bound L-Arg and serine 586 of G586S $nNOS_{oxy}$. The electron density map was calculated using Fourier coefficients $2F_o - F_c$, where F_o and F_c are the observed and calculated structure factors, respectively, the latter based on the final model. The contour level is 1σ, where σ is the rms electron density. (B) Overlay of G586S $nNOS_{oxy}$ (blue) and wild-type $nNOS_{oxy}$ (PDB ID 1OM4; grey). Hydrogen bonding interactions involving the side chain of serine 586 are shown as dotted lines. This figure was generated using PYMOL (The PyMOL Molecular Graphics System, Version 1.2r3pre, Schrödinger, LLC).

In the presence of NOHA, the G586S mutant formed an oxyferrous complex similar to that of the wild-type enzyme, with a Soret absorbance maximum at 424 nm. This decayed via a biphasic mechanism with rate-constants for oxyferrous decay slightly lower than those observed in the presence of L-Arg, and the final ferric heme species appeared to be mixed spin rather than the usual high spin form, with a Soret maximum at 400 nm. The intermediate spectrum formed in the presence of NOHA was a linear combination of the ferric and oxyferrous forms (see supplementary Figure S6). This indicates that it is unlikely to be a distinct species but may result from the oxyferrous complex decaying via two parallel kinetic routes. Oxyferrous decay in the presence of NOHA is complicated even in the WT enzyme by partial formation of the ferric nitrosyl complex as a precursor to NO release, and multiple phases are usually observed.

Crystal Structure of G586S $nNOS_{oxy}$: A data set to 2.6 Å resolution was used to refine the structure to a final *R*-factor of 19.87 % (R_{free} = 25.39 %; Table S1). The final model consists of the G586S nNOSoxy dimer. Subunit A consists of residues Arg299-Pro338 and Thr350-Trp716, while subunit B comprises residues Arg299-Pro338 and Val348-Gly718. Each subunit also contains one heme group, one bound H_4B molecule and one L-Arg substrate at the active site. In addition the model contains one Zn^{2+} ion in the dimer interface, and 196 water molecules. The rmsd fit of all backbone atoms for the wild-type (PDB ID 1OM4) and G586S nNOSoxy models is 0.3 Å, indicating no major differences between the two structures. The final $2F_o$-F_c electron density around Ser586 and the bound substrate (in subunit A) is shown in Figure 3. From the figure it can be seen that as a result of the G586S substitution there is an H-bonding interaction (3.0 Å) introduced between the serine side chain hydroxyl group and one of the substrate guanidinium N atoms. In addition, the S586 side chain hydroxyl is H-bonded to the backbone amide nitrogen of W587 (2.7 Å) and is 3.4 Å from the peptide oxygen of the same residue, consistent with a weak H-bonding interaction. All other interactions between the substrate and the active site are conserved in both the wild-type and G586S models.

Discussion

NO synthesis from L-arginine is an extraordinary chemical reaction involving the 5-electron oxidation of a guanidinium group by 2 equivalents of dioxygen. The reactions of a stable molecule such as L-arginine are generally limited to two-electron chemistry, in which electrons are transferred in pairs as covalent bonds are formed and broken. It is not easy to envisage how generation of the free radical NO from such a molecule could be achieved in an enzyme, and many possible mechanisms have been proposed [1-3, 24]. The reaction has been shown to take place in two steps, in each of which a molecule of dioxygen is activated on binding to the heme site in order to transform first L-arg to NOHA and then NOHA to NO and citrulline. The activation of dioxygen in NOS is similar to the process used by cytochromes P450 to initiate mono-oxygenation reactions. It is widely accepted that the active oxidant in these reactions is a highly unstable oxyferryl porphyrin radical cation species (compound I) [13-16] although this is not necessarily the active species in the NOS reactions. Compound I formation in a P450 requires 1-electron transfer to an Fe^{II}-O_2 complex, followed by two protonation steps and the loss of H_2O. In NOS the Fe^{II}-O_2 complex is formed in unusual circumstances, it is hydrogen-bonded to the guanidinium groups of either L-Arg or NOHA, which are both bound in their protonated states [37]. This electrostatic interaction is likely to be of mechanistic importance. The fact that it stabilises the oxyferrous complex significantly [23] indicates that the dioxygen molecule is polarised, such that electron density is shifted towards the distal oxygen, as in oxy-hemoglobin. In a P450 this is not usually the case and decay of the Fe^{II}-O_2 complex to Fe^{III} and superoxide can be much faster (up to 100 s^{-1}), although other factors also need to be taken into account [12]. Reduction of the Fe^{II}-O_2 complex in a P450 usually takes place via the transfer of a low-potential electron from a flavin or iron-sulfur cluster. In NOS, reduction occurs by electron transfer from H_4B and the situation is very different [1-3, 23, 24]. The H_4B cofactor is bound within hydrogen-bonding distance of one of the heme propionates. It is therefore close enough (5 Å away) to transfer an electron to the heme at approximately 10^{10} s^{-1} even with zero thermodynamic driving force [38]. However, H_4B is not a low potential reductant and the transfer of its electron to the Fe^{II}-O_2 complex is likely to be thermodynamically uphill. Thus, although the electron will be transferred rapidly, the equilibrium position of the electron transfer to the oxyferrous complex will disfavour reduction [39]. The rate of H_4B radical formation has been measured at 11 s^{-1} [40] at 10 °C, but this is too slow to be the fundamental rate of electron transfer and must be gated by a slow chemical step immediately preceding electron transfer. This process must then lock the electron in place by inducing immediate chemical decomposition. The obvious candidate for the slow step is protonation of the Fe^{II}-O_2 complex. It follows that this proton transfer event limits the rate of oxygen activation in NOS, in both steps of the catalytic reaction. The arrangement of H-bonds in the active site and the associated delivery of protons to dioxygen are therefore key aspects defining the reaction mechanism [3].

Figure 4 shows two possible mechanistic pathways for NO synthesis from L-Arg each based on different proton transfer events. For a discussion of bonding in the Fe^{II}-O_2 complex see Shaik and Chen [41]. In step 3a the thermodynamically unfavourable peroxo-heme complex removes a proton from the substrate to initiate the reaction as suggested by Zhu and Silverman [42]. In steps 2b and 3b the peroxo-heme complex captures a proton from the solvent to form a hydroperoxo-heme complex, before a second proton is captured, this time from the substrate guanidinium to initiate compound 1 formation. In both sides of the scheme the reaction is initiated by deprotonation of the guanidinium group. Deprotonation of the substrate is attractive because it generates an electron-rich nucleophilic species primed for reaction with the oxidising species in steps 4a or 4b [43]. Unlike step 4a, step 4b results in a direct bonding interaction between the newly formed NOHA and the heme iron, correlating with the observations of Davydov *et al*. [20].

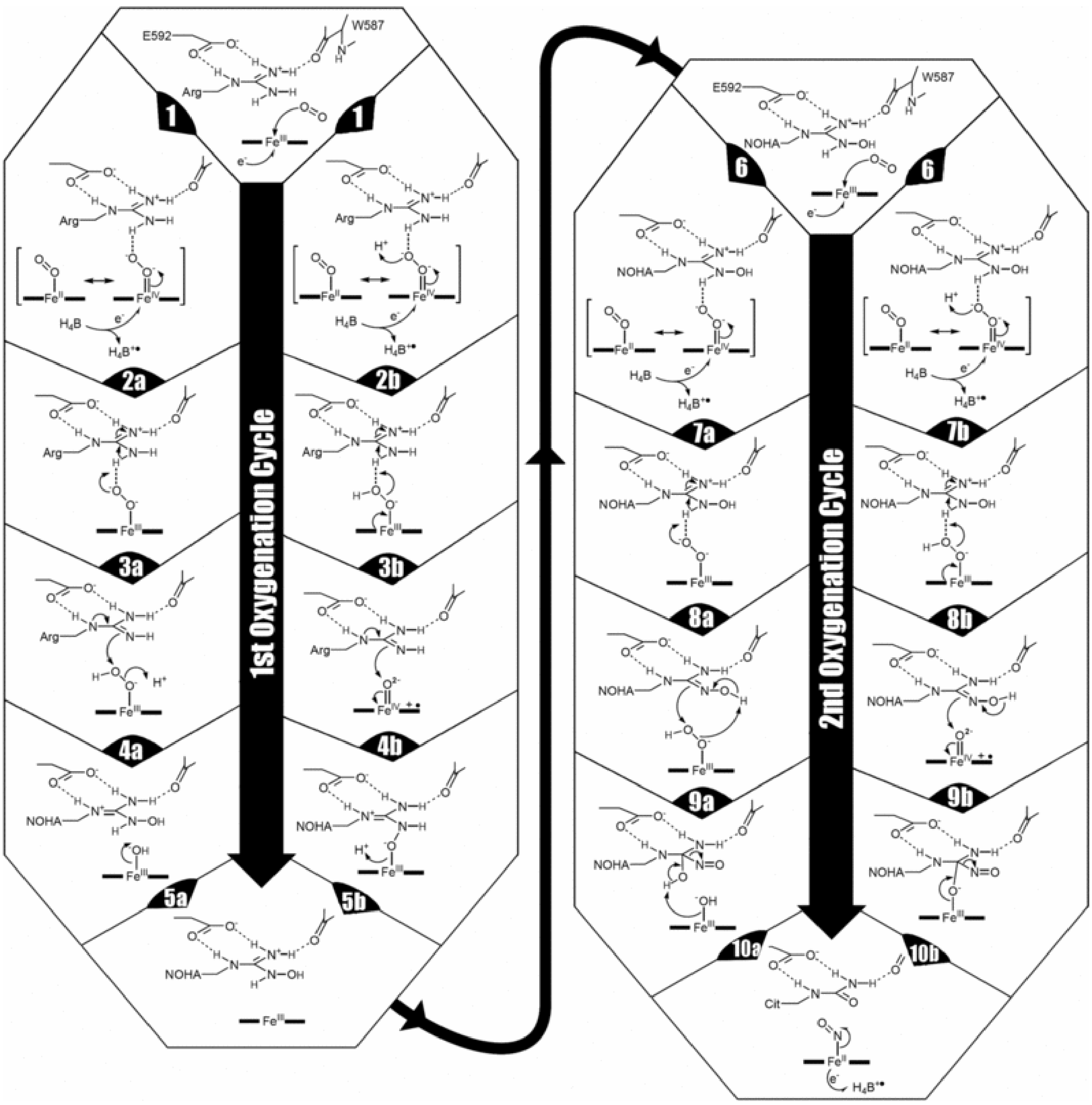

Figure 4. Comparison of Catalytic Reaction Mechanisms Proposed for NO Synthesis From L-Arg. The left side (a) shows a hydroperoxo heme species as the oxygenating agent, whereas the right side (b) shows formation of an oxyferryl radical cation (compound I).

The second oxygenation cycle shown in Figure 4 follows two paths similar to the those in the first cycle, which is logical because the substrates are both bound as guanidinium ions and interact similarly with bound dioxygen [23]. Divergence occurs in steps 9a and 9b where tetrahedral intermediates are formed from the guanidinium group. In 9b the intermediate is coordinated to the heme iron, whereas in 9a it is not. The first of these requires a substantial movement of the substrate away from its H-bonding environment (Glu592) towards the heme iron in order to make contact. This makes step 9b appear less likely, although the substrate has been deprotonated at this point and is no longer electrostatically attracted to Glu592. It is difficult to see why the compound I intermediate would form in the first cycle of catalysis, but not in the second, given the similarity of the substrates and active site environments. A recent DFT study of the second cycle indicated that compound I formation is the most favourable mechanistic route [44]. However, arguments in favour of different mechanisms for the two cycles have been proposed on the basis of the structures of the nitrosyl complexes of NOS [45]. Also, cryogenic EPR/ENDOR studies showed formation of a heme-bound product with L-Arg but not with NOHA [20, 46], favouring 9a. This latter study also followed the protonation of the heme oxygen complexes. In the presence of L-Arg protonation of the peroxo-complex appeared to occur before reaction, whereas in the presence of NOHA, the unprotonated peroxo species appeared to react. This subtle difference may indicate that the first reactive cycle requires two protons for oxygen activation, whereas the second requires only one. However, in both cases the substrate is likely to be deprotonated before oxygenation [47].

In order to resolve a mechanistic pathway for NOS, perturbing the active site environment to stabilise intermediates on the reaction pathway is a useful strategy. The G586S mutant described in this paper appears to have such an effect in the presence of L-Arg, but behaves differently with bound NOHA. In fact, with L-Arg, two unusual species are observed. The first is the Fe^{II}-O_2 complex, the Soret band of which is red-shifted significantly with respect to those of both the wild-type enzyme and aH_4B-bound mutant. The red-shift must result from the action of H_4B on the mutant Fe^{II}-O_2 complex i.e. electron transfer from H_4B to heme/oxygen, Step 2a of Figure 4. As discussed earlier, this is likely to be thermodynamically uphill, resulting in an equilibrium disfavouring electron transfer. In the mutant it is possible that the extra H-bond introduced by the G586S mutation acts to strengthen the H-bonding interaction between dioxygen and the guanidinium group, pulling the equilibrium over. The newly introduced Ser residue would therefore be acting as a proton donor during oxygen activation. The Fe^{II}-O_2 complex of the mutant may therefore contain significant hydroperoxoferric character. In support of this theory, the hydroperoxoferric heme complexes of P450s have similarly red-shifted Soret bands [48]. The second novel species observed is formed after decay of the oxyferrous complex. The UV/visible spectrum of this intermediate is unusual and may be an amalgamation of two or more species. However, it decays back to the ferric resting state in a single kinetic phase, with little ambiguity in the fitting process (see supplementary Figure S5). A mixture of two species would be expected to show biphasic decay with rate constants depending on the stability of each species (unless the two species exist in rapid equilibrium). The intermediate is formed after electron transfer from H_4B, so it is placed after step 2 in Figure 4. Possible candidates are therefore the peroxo- or hydroperoxo-heme complex formed in steps 2a and 3a, or the compound I species formed in step 3b. In P450 reactions, all of these are considered to be highly unstable. A recent paper by Rittle *et al.* [18] disentangles the UV/Vis spectra of these species and is useful for interpretation. The compound 1 species is characterised by a Soret band at around 370 nm and a long wavelength band at 680 nm. In some cases the porphyrin radical migrates to a nearby aromatic amino acid residue, as in the reaction of P450cam with peracids at low pH [49] which had a Soret maximum at 406 nm and a broad shoulder extending to 360 nm. Indeed, spectroscopic analysis of the NOS heme reaction with peroxy aceitic acid showed formation of a ferric heme species with coupling to an amino acid radical [50].The spectra of the compound I and ES species reported above have very little definition in the 500-600 nm region, unlike many other heme complexes. The intermediate observed in the reaction of G586S NOS_{oxy} with oxygen shares the lack of definition in this region and has significant absorption beyond 650 nm, in the Q-band region. It therefore most closely resembles a compound ES species. The NOS active site also contains a tetrahydrobiopterin radical cation, H-bonding to one of the heme propionates. In view of the unique properties of this heme site, the spectrum of the active oxygenating species in NOS is likely to be unusual. Tejero *et al.*, [51] reported the observation of a similar spectral intermediate during decay of the oxyferrous complex of W188H iNOSoxy in the presence of L-Arg, which mutates a residue stacking under the heme plane. The intermediate also had a Soret absorption maximum at 421 nm and was found to hydroxylate L-Arg.

The G586S intermediate reported here is unable to react with bound L-arg. The fact that it accumulates indicates that it has been stablised significantly by the G586S mutation. There are two possibilities to consider. Either the mutation alters the position of the substrate guanidinium group sufficiently to hinder its reaction with the species, or the additional H-bonding capability of the S586 residue stabilises the bound substrate sufficiently to hinder reaction (the intermediate may of course not be an active oxygenating species). We have no evidence that the substrate guanidinium group is bound in a modified position in the mutant crystal structure as compared to the wild type (Figure 3), and there is no reason to believe that this would be the case in the active complex. For a robust mechanism to have evolved, it seems unlikely that subtle changes in the position of the guanidinium group would derail the process. The effect of H-bonding between S586 and the substrate in the active site should therefore be considered. Figure 3 illustrates the likely H-bonds formed by S586. The serine side chain hydroxyl group is 3.0 Å and 3.5 Å from the terminal N groups of the guanidinium ion of the substrate, which must remain protonated. The S586 hydroxyl is therefore an H-bond acceptor from one of these. The hydroxyl is also an H-bond acceptor (2.7 Å) from the peptide NH of W587 and is 3.4 Å from the peptide oxygen of the same residue, so may therefore be a weak H-bond donor to this group. The net result is that S586 may be both an H-bond donor and acceptor to the system, thus stabilising substrate binding. The rate constants for the Fe^{II}-O_2 decay reaction are 2-fold slower for the mutant than wild-type nNOSoxy, indicating that the proton transfer(s) triggering decay of the complex and locking the electron in place are slowed by the mutation. i.e. Step 3b of Figure 4. A stronger H-bond between substrate and oxygen may slow down the transfer of the other proton in this case. Step 4 (a or b) in Figure 4 involves reaction of the deprotonated guanidine group with the activated oxy-heme complex. In the mutant, deprotonation of the substrate will induce a rearrangement of the H-bonds in the active site pocket. The S586 hydroxyl group will become an H-bond donor to the substrate, stabilising it by reprotonation, and possibly by limiting motion of the substrate towards the reactive oxygenating complex (Figure 5). This would be expected to hinder Step 4 of the reaction, which requires a nucleophilic/electron rich substrate to move towards and react with an electron deficient oxyheme complex. Thus, the G586S mutant may stabilise the active oxygenating species by supplying an additional proton at a key stage of the reaction. As shown by de Visser and Tan [43], the protonated substrate is a less effective reactant than the deprotonated form. It is possible that the guanidinium group is not sufficiently reactive to undergo transformation before the active oxygenating species decays. For iNOSoxy, the H_4B radical decays at 0.71 s^{-1} [40] after hydroxylation of L-Arg. Decay of the G586S nNOSoxy intermediate occurs at a similar rate, perhaps via reductive electron transfer from the H_4B radical cation.

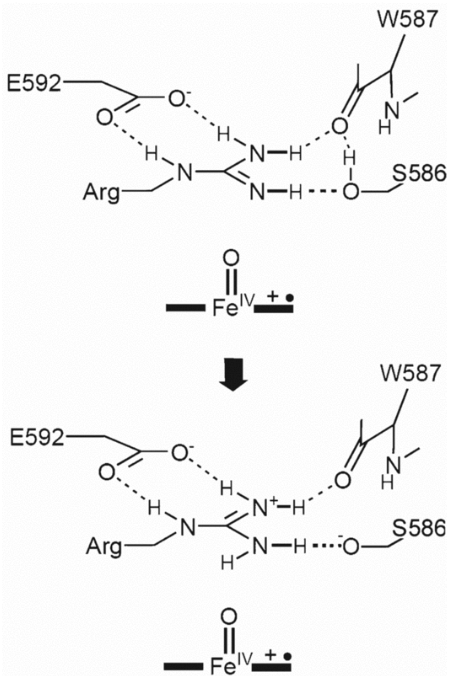

Figure 5. Possible interactions between bound substrate and Ser586 during Step 4 of the oxygen activation process.

The additional H-bond to the substrate guanidinium group in the active site of NOS provided by the G586S mutation offers a subtle perturbation to the mechanistic pathway followed, and specifically probes the role of proton transfer. It uniquely enables the mutant to distinguish between the two substrates, supporting evidence that LArg requires deprotonation prior to monoxygenation by a compound 1 type species, whereas NOHA is able to be transformed even when protonated. Consequently NOS appears to follow the *b* side of Fig.6 during the first monooxygenation cycle, but the *a* side during the second.

References

[1] Daff, S. (2010) NO synthase: Structures and mechanisms. *Nitric Oxide-Biology and Chemistry.* **23**, 1-11.

[2] Stuehr, D. J., Santolini, J., Wang, Z. Q., Wei, C. C. and Adak, S. (2004) Update on mechanism and catalytic regulation in the NO synthases. *Journal of Biological Chemistry*. **279**, 36167-36170.

[3] Santolini, J. (2011) The molecular mechanism of mammalian NO-synthases: A story of electrons and protons. *Journal of Inorganic Biochemistry.* **105**, 127-141.

[4] Alderton, W. K., Cooper, C. E. and Knowles, R. G. (2001) Nitric oxide synthases: structure, function and inhibition. *Biochemical Journal.* **357**, 593-615.

[5] Crane, B. R., Arvai, A. S., Ghosh, D. K., Wu, C. Q., Getzoff, E. D., Stuehr, D. J. and Tainer, J. A. (1998) Structure of nitric oxide synthase oxygenase dimer with pterin and substrate. *Science*. **279**, 2121-2126.

[6] Raman, C. S., Li, H. Y., Martasek, P., Kral, V., Masters, B. S. S. and Poulos, T. L. (1998) Crystal structure of constitutive endothelial nitric oxide synthase: A paradigm for pterin function involving a novel metal center. *Cell*. **95**, 939-950.

[7] Garcin, E. D., Bruns, C. M., Lloyd, S. J., Hosfield, D. J., Tiso, M., Gachhui, R., Stuehr, D. J., Tainer, J. A. and Getzoff, E. D. (2004) Structural basis for isozyme-specific regulation of electron transfer in nitric-oxide synthase. *Journal of Biological Chemistry.* **279**, 37918-37927.

[8] Roman, L. J., Martasek, P. and Masters, B. S. S. (2002) Intrinsic and extrinsic modulation of nitric oxide synthase activity. *Chemical Reviews.* **102**, 1179-1189.

[9] Adak, S., Wang, Q. and Stuehr, D. J. (2000) Arginine conversion to nitroxide by tetrahydrobiopterin-free neuronal nitric-oxide synthase - Implications for mechanism. *Journal of Biological Chemistry.* **275**, 33554-33561.

[10] Wei, C. C., Wang, Z. Q., Hemann, C., Hille, R. and Stuehr, D. J. (2003) A tetrahydrobiopterin radical forms and then becomes reduced during N-omega-hydroxyarginine oxidation by nitric-oxide synthase. *Journal of Biological Chemistry.* **278**, 46668-46673.

[11] Adak, S., Crooks, C., Wang, Q., Crane, B. R., Tainer, J. A., Getzoff, E. D. and Stuehr, D. J. (1999) Tryptophan 409 controls the activity of neuronal nitric-oxide synthase by regulating nitric oxide feedback inhibition. *Journal of Biological Chemistry.* **274**, 26907-26911.

[12] Ost, T. W. B., Clark, J., Mowat, C. G., Miles, C. S., Walkinshaw, M. D., Reid, G. A., Chapman, S. K. and Daff, S. (2003) Oxygen activation and electron transfer in flavocytochrome P450BM3. *Journal of the American Chemical Society.* **125**, 15010-15020.

[13] Bollinger, J. M. and Krebs, C. (2006) Stalking intermediates in oxygen activation by iron enzymes: Motivation and method. *Journal of Inorganic Biochemistry.* **100**, 586-605.

[14] Denisov, I. G., Makris, T. M., Sligar, S. G. and Schlichting, I. (2005) Structure and chemistry of cytochrome P450. *Chemical Reviews.* **105**, 2253-2277.

[15] Koppenol, W. H. (2007) Oxygen activation by cytochrome P450: A thermodynamic analysis. *Journal of the American Chemical Society.* **129**, 9686-9690.

[16] Meunier, B., de Visser, S. P. and Shaik, S. (2004) Mechanism of oxidation reactions catalyzed by cytochrome P450 enzymes. *Chemical Reviews.* **104**, 3947-3980.

[17] Kellner, D. G., Hung, S. C., Weiss, K. E. and Sligar, S. G. (2002) Kinetic characterization of Compound I formation in the thermostable cytochrome P450 CYP119. *Journal of Biological Chemistry.* **277**, 9641-9644.

[18] Rittle, J. and Green, M. T. (2010) Cytochrome P450 Compound I: Capture, Characterization, and C-H Bond Activation Kinetics. *Science*. **330**, 933-937.

[19] Davydov, R., Makris, T. M., Kofman, V., Werst, D. E., Sligar, S. G. and Hoffman, B. M. (2001) Hydroxylation of camphor by-reduced oxy-cytochrome P450cam: Mechanistic implications of EPR and ENDOR studies of catalytic intermediates in native and mutant enzymes. *Journal of the American Chemical Society.* **123**, 1403-1415.

[20] Davydov, R., Ledbetter-Rogers, A., Martasek, P., Larukhin, M., Sono, M., Dawson, J. H., Masters, B. S. S. and Hoffman, B. M. (2002) EPR and ENDOR characterization of intermediates in the cryoreduced oxy-nitric oxide synthase heme domain with bound L-arginine or N-G-hydroxyarginine. *Biochemistry*. **41**, 10375-10381.

[21] Hurshman, A. R., Krebs, C., Edmondson, D. E., Huynh, B. H. and Marletta, M. A. (1999) Formation of a pterin radical in the reaction of the heme domain of inducible nitric oxide synthase with oxygen. *Biochemistry*. **38**, 15689-15696.

[22] Bec, N., Gorren, A. C. F., Voelker, C., Mayer, B. and Lange, R. (1998) Reaction of neuronal nitric-oxide synthase with oxygen at low temperature - Evidence for reductive activation of the oxy-ferrous complex by tetrahydrobiopterin. *Journal of Biological Chemistry.* **273**, 13502-13508.

[23] Ost, T. W. B. and Daff, S. (2005) Thermodynamic and kinetic analysis of the nitrosyl, carbonyl, and dioxy heme complexes of neuronal nitric-oxide synthase - The roles of substrate and tetrahydrobiopterin in oxygen activation. *Journal of Biological Chemistry.* **280**, 965-973.

[24] Crane, B. R., Sudhamsu, J. and Patel, B. A. (2010) Bacterial Nitric Oxide Synthases. Annual *Review of Biochemistry.* **79**, 445-470.

[25] Sagami, I., Daff, S. and Shimizu, T. (2001) Intra-subunit and inter-subunit electron transfer in neuronal nitric-oxide synthase - Effect of calmodulin on heterodimer catalysis. Journal of *Biological Chemistry.* **276**, 30036-30042.

[26] Kunkel, T. A. (1985) RAPID AND EFFICIENT SITE-SPECIFIC MUTAGENESIS WITHOUT PHENOTYPIC SELECTION. *Proceedings of the National Academy of Sciences of the United States of America.* **82**, 488-492.

[27] Sagami, I. and Shimizu, T. (1998) The crucial roles of Asp-314 and Thr-315 in the catalytic activation of molecular oxygen by neuronal nitric-oxide synthase - A site-directed mutagenesis study. *Journal of Biological Chemistry.* **273**, 2105-2108.

[28] Ghosh, D. K., Holliday, M. A., Thomas, C., Weinberg, J. B., Smith, S. M. E. and Salerno, J. C. (2006) Nitric-oxide synthase output state - Design and properties of nitric-oxide synthase oxygenase/FMN domain constructs. *Journal of Biological Chemistry.* **281**, 14173-14183.

[29] Woodward, J. J., Chang, M. M., Martin, N. I. and Marletta, M. A. (2009) The Second Step of the Nitric Oxide Synthase Reaction: Evidence for Ferric-Peroxo as the Active Oxidant. *Journal of the American Chemical Society.* **131**, 297-305.

[30] Smith, S. M. E., Sham, C., Roman, L., Martasek, P. and Salerno, J. C. (2001) Titration of low K-d binding sites : Binding of arginine analogs to nitric oxide synthases. *Nitric Oxide-Biology and Chemistry.* **5**, 442-452.

[31] AbuSoud, H. M., Presta, A., Mayer, B. and Stuehr, D. J. (1997) Analysis of neuronal NO synthase under single-turnover conditions: Conversion of N-omega-hydroxyarginine to nitric oxide and citrulline. *Biochemistry*. **36**, 10811-10816.

[32] Collaborative Computational Project, N. (1994) The CCP4 Suite: Programs for protein crystallography. *Acta Crystallographica Section D Biological Crystallography.* **50**, 760-763.

[33] Emsley, P. and Cowtan, K. (2004) Coot: model-building tools for molecular graphics. *Acta Crystallographica Section D-Biological Crystallography.* **60**, 2126-2132.

[34] Adams, P. D., Grosse-Kunstleve, R. W., Hung, L. W., Ioerger, T. R., McCoy, A. J., Moriarty, N. W., Read, R. J., Sacchettini, J. C., Sauter, N. K. and Terwilliger, T. C. (2002) PHENIX: building new software for automated crystallographic structure determination. *Acta Crystallographica Section D-Biological Crystallography.* **58**, 1948-1954.

[35] Li, H. Y., Shimizu, H., Flinspach, M., Jamal, J., Yang, W. P., Xian, M., Cai, T. W., Wen, E. Z., Jia, Q. A., Wang, P. G. and Poulos, T. L. (2002) The novel binding mode of N-Alkyl-N '-hydroxyguanidine to neuronal nitric oxide synthase provides mechanistic insights into NO biosynthesis. *Biochemistry*. **41**, 13868-13875.

[36] Wei, C. C., Crane, B. R. and Stuehr, D. J. (2003) Tetrahydrobiopterin radical enzymology. *Chemical Reviews.* **103**, 2365-2383.

[37] Crane, B. R., Arvai, A. S., Ghosh, S., Getzoff, E. D., Stuehr, D. J. and Tainer, J. A. (2000) Structures of the N-omega-hydroxy-L-arginine complex of inducible nitric oxide synthase oxygenase dimer with active and inactive pterins. *Biochemistry*. **39**, 4608-4621.

[38] Moser, C. C., Keske, J. M., Warncke, K., Farid, R. S. and Dutton, P. L. (1992) NATURE OF BIOLOGICAL ELECTRON-TRANSFER. *Nature*. **355**, 796-802.

[39] Groves, J. T. and Wang, C. C. Y. (2000) Nitric oxide synthase: models and mechanisms. *Curr. Opin. Chem. Biol.* **4**, 687-695.

[40] Wei, C. C., Wang, Z. Q., Wang, Q., Meade, A. L., Hemann, C., Hille, R. and Stuehr, D. J. (2001) Rapid kinetic studies link tetrahydrobiopterin radical formation to heme-dioxy reduction and arginine hydroxylation in inducible nitric-oxide synthase. *Journal of Biological Chemistry.* **276**, 315-319.

[41] Shaik, S. and Chen, H. (2011) Lessons on O(2) and NO bonding to heme from ab initio multireference/multiconfiguration and DFT calculations. *J. Biol. Inorg. Chem.* **16**, 841-855.

[42] Zhu, Y. Q. and Silverman, R. B. (2008) Revisiting heme mechanisms. a perspective on the mechanisms of nitric oxide synthase (NOS), heme oxygenase (HO), and cytochrome p450s (CYP450s). *Biochemistry*. **47**, 2231-2243.

[43] de Visser, S. P. and Tan, L. S. (2008) Is the bound substrate in nitric oxide synthase protonated or neutral and what is the active oxidant that performs substrate hydroxylation? *Journal of the American Chemical Society.* **130**, 12961-12974.

[44] Robinet, J. J., Cho, K.-B. and Gauld, J. W. (2008) A density functional theory investigation on the mechanism of the second half-reaction of nitric oxide synthase. *Journal of the American Chemical Society.* **130**, 3328-3334.

[45] Pant, K. and Crane, B. R. (2006) Nitrosyl-heme structures of Bacillus subtilis nitric oxide synthase have implications for understanding substrate oxidation. *Biochemistry*. **45**, 2537-2544.

[46] Davydov, R., Sudhamsu, J., Lees, N. S., Crane, B. R. and Hoffman, B. M. (2009) EPR and ENDOR Characterization of the Reactive Intermediates in the Generation of NO by Cryoreduced Oxy-Nitric Oxide Synthase from Geobacillus stearothermophilus. *Journal of the American Chemical Society.* **131**, 14493-14507.

[47] Giroud, C., Moreau, M., Mattioli, T. A., Balland, V., Boucher, J. L., Yun, X. L., Stuehr, D. J. and Santolini, J. (2010) Role of Arginine Guanidinium Moiety in Nitric-oxide Synthase Mechanism of Oxygen Activation. *Journal of Biological Chemistry.* **285**, 7233-7245.

[48] Sligar, S. G., Makris, T. M. and Denisov, I. G. (2005) Thirty years of microbial P450 monooxygenase research: Peroxo-heme intermediates - The central bus station in heme oxygenase catalysis. *Biochem. Biophys. Res. Commun.* **338**, 346-354.

[49] Spolitak, T., Dawson, J. H. and Ballou, D. P. (2005) Reaction of ferric cytochrome P450cam with peracids - Kinetic characterization of intermediates on the reaction pathway. *Journal of Biological Chemistry.* **280**, 20300-20309.

[50] Jung, C., Lendzian, F., Schunemann, V., Richter, M., Bottger, L. H., Trautwein, A. X., Contzen, J., Galander, M., Ghosh, D. K. and Barra, A. L. (2005) Multi-frequency EPR and Mossbauer spectroscopic studies on freeze-quenched reaction intermediates of nitric oxide synthase. *Magn. Reson. Chem.* **43**, S84-S95.

[51] Tejero, J. S., Biswas, A., Wang, Z.-Q., Page, R. C., Haque, M. M., Hemann, C., Zweier, J. L., Misra, S. and Stuehr, D. J. (2008) Stabilization and Characterization of a Heme-Oxy Reaction Intermediate in Inducible Nitric-oxide Synthase. *Journal of Biological Chemistry.* **283**, 33498-33507.